Adsorption and capillary condensation of ^{4}He on Nuclepore: Third-sound and capacitance measurements

D. T. Smith, K. M. Godshalk, and R. B. Hallock
Laboratory for Low Temperature Physics, Department of Physics and Astronomy, University of Massachusetts, Amherst, Massachusetts 01003
(Received 21 January 1987)

The adsorption of ^{4}He films on Nuclepore filter materials of several pore sizes has been studied for temperatures in the range $1.4\ \text{K} \lesssim T \lesssim 1.8\ \text{K}$ using simultaneous measurements of the time of flight of pulsed third sound and capacitance measurements of the mass of ^{4}He in the pores. The third-sound and capacitance data for values of the film thickness $4 < h(\text{layers}) < 25$, which span capillary condensation of the pores, show strongly hysteretic behavior. Correlations between the third-sound and capacitance data aid in understanding the film configuration(s) for a given value of the helium film thickness. Good agreement is found between the capacitance data and the theory which describes the behavior of helium films in cylindrical geometries due to Saam and Cole, if a distribution in pore radii is assumed. Good agreement is also found between the third-sound time-of-flight data and the theory of Cohen, Guyer, and Machta which describes the velocity of third sound on Nuclepore. The nature of the Kosterlitz-Thouless transition in the ^{4}He film is briefly explored on both porous Nuclepore and a sample of the substrate material without holes.

I. INTRODUCTION

In this paper we describe experiments which seek to explore the behavior of helium films on the disordered polycarbonate substrate Nuclepore.[1] Our motivation for these experiments comes from two directions. To prepare for NMR and third-sound experiments in thin ^{3}He-^{4}He mixture films on these substrates we require a detailed knowledge of the behavior of pure ^{4}He films on them. Our second motivation has been the desire to characterize and understand in some detail the nature of hysteretic capillary condensation. Nuclepore, with its nominally cylindrical and relatively uniform pores appeared to be a suitable substrate for such studies.

We will report here detailed studies of the propagation of third sound as a function of the helium film thickness on two Nuclepore samples of characteristic pore diameter 800 and 2000 Å. The third-sound velocity is found[2] to be a hysteretic function of the film thickness and this is explained on the basis of a simple model of capillary condensation in the pores. An unexpected propagation is observed when the pores are fully capillary condensed. The model proposed by Cohen *et al.*[3] to explain earlier data[2] is found to be in general agreement with our current measurements. Direct measurements of the amount of helium adsorbed onto the substrate as a function of film thickness are made by means of capacitance techniques and the hysteretic behavior observed is found to correlate directly with the third sound measurements. Taken together the two sets of measurements allow a detailed interpretation of the morphology of the helium coverage and a direct measure of the pore size distribution for the Nuclepore. We will conclude with measurements of the velocity of third sound in the vicinity of the Kosterlitz-Thouless[4] transition. The transition region appears to be sharper on the porous Nuclepore than it is on a sample of the same substrate material which has no pores.

We begin in Sec. II with a discussion of the relevant theory of third sound and a discussion of the hydrodynamics. Capillary condensation is discussed in the context of the theory of Saam and Cole.[5] In Sec. III we describe the experimental details and report results for both the third sound and capacitance measurements.

II. THIRD SOUND AND CAPILLARY CONDENSATION IN CYLINDRICAL GEOMETRIES

A. Nuclepore substrates

The Nuclepore[1] filter materials used were porous polycarbonate sheets manufactured by Nuclepore Corporation by use of an irradiation and etching process. The technique produces narrow, relatively straight cylindrical pores with a reasonably narrow distribution of pore radii oriented at angles $\theta \lesssim 34°$ from the perpendicular to the plane of the sheet as shown schematically in Fig. 1.

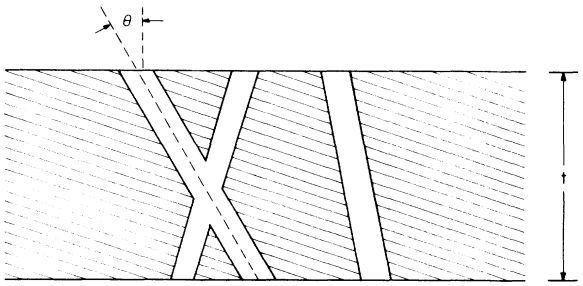

FIG. 1. Schematic illustration of a cross section (perpendicular to the plane) of Nuclepore filter material. Because of the pore diameter, the areal density of the pores, and the average of the angle, θ, that the pores make with a normal to the surface, many of the pores intersect at least one other pore somewhere along their length.

TABLE I. Nominal specifications for the Nuclepore used in these measurements.

Pore diameter (Å)	Filter thickness, t (μm)	Pore density, ξ (cm^{-2})
800	6	6×10^8
2000	10	3×10^8

Manufacturer's specifications for the two pore sizes used in these experiments are given in Table I. In addition to the porous samples, a piece of virgin polycarbonate was obtained from the manufacturer and was used as a reference third sound substrate. Scanning electron microscope (SEM) photographs of both the surface and a microtome cross section perpendicular to the plane of 2000-Å Nuclepore, taken after the sputtering of ~200 Å of Pt onto the surface, are shown in Fig. 2.

The well-defined geometry and the small pore sizes of Nuclepore filters have made the filters a good substrate for studying the properties of ^{4}He films in confined geometries. Gasparini and coworkers have chosen 2000-Å Nuclepore as the substrate on which to study finite-size effects on the superfluid transition in ^{4}He films. They have carried out adsorption measurements[6] on 2000-Å Nuclepore which reveal the first and second-layer completion using Langmuir and Brunauer, Emmett, and Tetter (BET) analyses[7] of the data. This analysis yields a surface area of 1.5 times the expected geometric surface area deduced from the manufacturer's specifications. Measurements of the specific heat[6] of ^{4}He films adsorbed on Nuclepore show two thermodynamic transitions for helium film thicknesses of seventeen atomic layers or greater. Both transition temperatures are below the bulk λ transition, presumably due to the finite-size effects induced by the Nuclepore. Two transitions can be explained on the basis of an instability for cylindrical pores predicted by Saam and Cole[5] and discussed in detail below. The film geometry which occurs at the instability is shown in Fig. 3(II); the helium which bridges the pore diameter should have a higher transition temperature than the helium film.

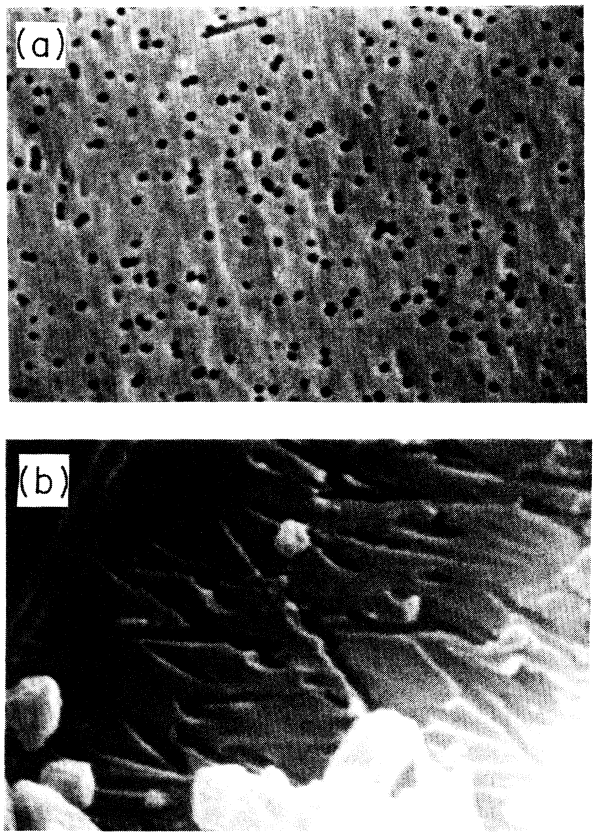

FIG. 2. Scanning electron microscope pictures of (a) the surface and (b) the cross section of a 2000-Å Nuclepore sample prepared by low-temperature microtome. Both pictures were taken after sputtering ~200 Å of Pt onto the surfaces. Samples were also prepared with 500, 1000, and 1500 Å of Ag evaporated onto the surface; measurements of the pore opening dimensions for these samples showed that the Ag did not measurably decrease the diameter of the pore openings.

Nuclepore filters have also proven to be an interesting system with which to study the bulk superfluid transition of ^{4}He and ^{3}He-^{4}He mixtures in confined geometries. Thomlinson *et al.*[8] have used Nuclepore as a superleak second sound transducer to study the superfluid transition in bulk ^{3}He-^{4}He mixtures. Brooks *et al.*[9] have observed a suppressed ^{4}He superfluid density for ^{4}He in Nuclepore pores by measuring the pressure difference across a filter membrane which is part of a Helmholtz resonator.

In all of the work described above, the reasonably well-defined geometry of the Nuclepore pores has been a major factor in the phenomenon studied. Nuclepore was chosen for the current studies in part because of its apparent relatively simple geometry.

B. Equations of third sound

Third sound in helium films is analogous to tidal waves on water; the wavelengths involved are much longer than the depth of the medium. The velocity C in each case is given to good approximation by $C=\sqrt{fh}$, where h is the thickness of the medium and f is the restoring force per unit mass. For tidal waves, this force is gravity; for third sound waves, the restoring force is the van der Waals attraction between a ^{4}He atom and the substrate. In general,[10,11] that force is given by

$$f=\frac{\alpha\beta(3\beta+4h)}{h^4(h+\beta)^2}\ , \tag{1}$$

where α is the van der Waals constant for the helium-substrate interaction and β is a parameter used to describe retardation effects which become important at thicker coverages.[11] These retardation effects cause the potential to change from a $1/h^3$ to a $1/h^4$ dependence for thick helium films.[11] The full third sound velocity C_3, with the inclusion of temperature-dependent terms,[12,13] is given by

$$C_3^2=\frac{\langle\rho_s\rangle}{\rho}\left[1+\frac{TS}{L}\right]^2\frac{\alpha\beta(3\beta+4h)}{h^3(h+\beta)^2}\ , \tag{2}$$

where $\langle\rho_s\rangle/\rho$ is the average superfluid density in the film, T is the temperature, S is the entropy, and L is the latent

heat. Over the temperature range of interest, here 1.4 K $\lesssim T \lesssim$ 1.8 K, the average superfluid density in the film has been measured[12] and obeys the empirical relation $\langle \rho_s \rangle / \rho = (\rho_s/\rho)(1 - D/h)$, where ρ_s/ρ is the bulk superfluid density and D is a temperature-dependent parameter which describes the amount of "fixed" or "solid" helium in the film. For very thin films ($h \lesssim 10$ atomic layers, where 1 atomic layer = 3.6 Å), retardation effects are negligible and the restoring force can be approximated by $f = 3\alpha/h^3$, so that the velocity becomes

$$C_3^2 \approx \frac{\langle \rho_s \rangle}{\rho} \frac{3\alpha}{h^3} \left[1 + \frac{TS}{L} \right]^2 . \tag{3}$$

The parameter D can be determined experimentally by measuring the third sound velocity as a function of h at thin coverages and rearranging the simplified velocity expression to read

$$\Gamma = h - D = \frac{C_3^2 h^4 \rho}{3\alpha \rho_s (1 + TS/L)^2} . \tag{4}$$

A plot of Γ versus h has an intercept D. $D(T)$ has been determined for helium on glass[12] and other substrates.[14]

In order to develop a theory to describe the propagation of third sound on Nuclepore, it is first necessary to examine the effects of the cylindrical geometry on the configuration of the film inside the pore. The adsorption of a helium film in a cylindrical pore is discussed in the next section, and the propagation of third sound on Nuclepore will be examined in Sec. II D.

C. Saam and Cole theory

The hydrodynamic and thermodynamic properties of ^{4}He films adsorbed in cylindrical pores have been calculated by Saam and Cole[5] (SC). They determine the film thickness at which it is energetically favorable for a pore to capillary condense rather than have a uniform thick film adsorbed on the walls. A region in which the film configuration is metastable is also found; this provides a probable explanation for the hysteresis typically observed in the adsorption isotherms of porous media. Since Nuclepore is composed of roughly cylindrical pores, the theory of SC can be applied to the adsorption of liquid helium in Nuclepore, if one ignores intersections of the pores. Recent adsorption isotherm measurements in porous glasses prepared by a sol-gel technique[15] are in good agreement with the theory of Saam and Cole.

To model the adsorbed film, SC assume van der Waals forces between the substrate and film, in contrast to the classical Kelvin theory,[16] which ignores substrate interactions. The van der Waals potential for cylindrical geometry can be calculated by assuming the potential is a sum of pair interactions of the form $-c/r^6$. Such a calculation has been carried out by SC, with the result for the van der Waals potential $U(A)$:

$$U(A) = -\frac{3\pi\alpha}{2R^3} F(3/2, 5/2; 1; Y^2) , \tag{5}$$

where R is the radius of the cylindrical pore, $Y = A/R$, A is the inner *radius* to the film surface as measured from the center of the pore (Fig. 3), α is the van der Waals constant, and F is a hypergeometric function. The adsorbed film is assumed to have a mass density which varies rapidly over the first few layers near the wall, and is uniform throughout the remainder of the fluid. The first layer or so near the substrate is strongly bound and does not participate in the superfluid motion.

SC use the equations of quantum hydrodynamics for an ideal compressible fluid and the above model for the adsorbed film to calculate the spectrum of fluid excitations for helium films in a cylindrical pore. Two oscillatory modes are found; one is a surface wave in which the fluid motion is confined to the vicinity of the liquid-vapor interface, and the other is a sound wave involving fluid motion throughout the liquid. For sufficiently thin films the surface modes will dominate. If a free surface is present, the mode is third sound as discussed above; in the absence of a free surface the mode is fourth sound. In the hydrodynamic calculation a temperature of $T = 0$ is assumed, but this restriction is removed in a later thermodynamic calculation which gives the same results as the $T = 0$ case.

When one begins with an empty pore and starts to add helium atoms, the film will reside in configuration I, shown in Fig. 3. In configuration I the film coats the walls of the pore with an inner film radius of A. When the film radius reaches A_m, configuration I becomes metastable relative to configuration II (Fig. 3), in the sense that configuration II has a lower free energy, but may only be reached by a macroscopic deformation of configuration I. The metastable film radius A_m is determined by minimizing the free energy for a fixed number of particles; the result, given in terms of the scaling parameter R_0 is

$$\frac{3\pi\alpha}{R_0^2} = -A_m U(A_m) + \frac{2}{A_m} \int_0^{A_m} A U(A) dA . \tag{6}$$

R_0 is given by $R_0^2 = 3\pi\alpha/\sigma v_l$, where σ is the surface tension of ^{4}He, $v_l = M_4/\rho$, M_4 is the mass of the ^{4}He atom

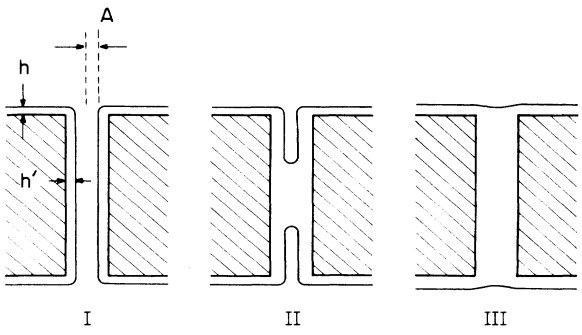

FIG. 3. Three possible film configurations in the pores. In configuration I the film thickness h' in the pore is somewhat larger than the film thickness h on the flat surface due to surface tension. The dimension A is the radius of the film surface in the pore. Configuration II represents a film profile which could occur when a portion of the pore is condensed. Because of pore intersections and imperfections in the pores, actual condensed regions could have a much more complicated geometry. In configuration III the pore is completely condensed.

and ρ is the liquid density.

As one continues to add atoms the film radius will decrease past the radius A_m. In this region, configuration II is still not accessible without some perturbation being applied to the film in configuration I. The film will remain in configuration I until the film radius A_c is reached. At this point the hydrodynamics reveal a long-wavelength instability in the surface modes for configuration I. The instability occurs when the mode frequency becomes imaginary, and the film radius A_c at the instability is given by

$$\left.\frac{dU(A)}{dA}\right|_{A=A_c} = \frac{v_l\sigma}{A_c^2} \ . \tag{7}$$

At the film radius A_c it is no longer possible for the film to remain in configuration I, and the pore will fill, as shown in Fig. 3(III).

The above argument for the film radius A_c at condensation is valid only for $T=0$. To remove this restriction, SC examine the thermodynamics of a film adsorbed in a cylindrical pore. The thermodynamic argument begins with the equilibrium between the vapor and the film of radius A inside a pore. The equilibrium pressures P_v and P_l of the vapor and film are related by

$$P_v = P_l + \frac{\sigma}{A} \ . \tag{8}$$

Employing the Gibbs-Duhem relation $d\mu = VdP$ for constant T will then give the chemical potentials μ_l and μ_v for the liquid and vapor in terms of their value at the saturated vapor pressure P_0. The chemical potential of the system is found by equating μ_l and μ_v, to get

$$\mu = \mu_0(P_0,T) + U(A) - \frac{v_l\sigma}{A} \ . \tag{9}$$

Thermodynamic stability requires that $\partial\mu/\partial N \geq 0$, where N is the number of particles. Increasing the number of particles corresponds to decreasing the film radius A, so that combining the stability requirement and Eq. (9) will give Eq. (7) for arbitrary T.

Substituting Eq. (5) for the van der Waals potential, and using the fact that

$$\frac{d}{dz}F(a,b;c;z) = \frac{ab}{c}F(a+1,b+1;c+1;z)$$

in Eqs. (6) and (7) gives for the instabilities Y_m and Y_c

$$\frac{R^2}{R_0^2} = \frac{Y_m}{2}F(\tfrac{3}{2},\tfrac{5}{2};1;Y_m^2) - \frac{1}{Y_m}\int_0^{Y_m} YF(\tfrac{3}{2},\tfrac{5}{2};1;Y^2)dY \ , \tag{10}$$

$$\frac{R^2}{R_0^2} = \frac{15}{4}Y_c^3F(\tfrac{5}{2},\tfrac{7}{2};2;Y_c^2) \ . \tag{11}$$

The above results can be used to calculate adsorption isotherms in cylindrical pores. The filling fraction X for a collection of pores of radius R with the film in configuration I is

$$X = (R^2 - A^2)/R^2 = 1 - Y^2 \tag{12}$$

assuming ideal parallel pores. Here $A = RY$ is the inner radius of the film surface. The reduced pressure is given by

$$p = \frac{P}{P_0} = \exp\left[-\left[U(A) + \frac{\sigma v_l}{A}\right]\Big/ k_BT\right] \ , \tag{13}$$

and the filling fraction as a function of pressure is found numerically from Eqs. (12) and (13). In an adsorption experiment conducted as a function of increasing pressure the pores will remain in the metastable configuration I until $A = A_c$, at which point the pores will begin to fill at constant pressure. The pressure at the instability (metastability) is found by substituting $Y = Y_c (Y = Y_m)$ in Eq. (13). At P_c the function $X(p)$ has an infinite derivative, so the pores will fill at constant pressure. Once the pore is full, any further increase in pressure will only increase the film thickness on the flat surface. To empty the condensed pores, the pressure must be reduced to the pressure P_m corresponding to the lower limit in pressure of the metastable region before the pores will go to configuration II and begin to empty. The expression for A_m is independent of the number of particles present, indicating that, as particles are taken away, the curved meniscus will move so as to reduce the condensed volume at a constant chemical potential, or constant pressure. Once the pressure is reduced to P_m, the pores will empty at constant pressure until the film goes to configuration I, with $A = A_m$, after which further desorption will be governed by Eq. (13).

D. Cohen-Guyer-Machta theory

Cohen, Guyer, and Machta[3] (CGM) have considered the properties of ^{4}He films adsorbed in cylindrical pores with an emphasis on understanding the propagation of third sound on Nuclepore. Because the wavelengths of third sound involved (≥ 1 mm) are much longer than the spacing between pores (~ 1 μm) and the length of the pores (~ 10 μm), CGM take a coarse-grained approach in describing the effect of the pores on third sound. They predict the sound speed for two different configurations of film in the pores—the case where the film lines the pores but does not bridge the diameter anywhere [Fig. 3(I)], and the case where the pores are completely filled [Fig. 3(III)]. By examining the hydrodynamic modes of the superfluid for the pore and flat-surface system, they arrive at an expression for the velocity of sound C on a Nuclepore filter

$$C^2 = \left[n_s + \frac{n_p}{\epsilon}\right]\left[\frac{n_s}{C_4^2} + \frac{n_s}{C_3^2} + \frac{n_p}{C_p^2}\right]^{-1} \ , \tag{14}$$

where n_s (n_p) is the areal density of the film on the surface (in the pores), C_3 (C_4) is the third (fourth) sound velocity, C_p is the sound speed in a pore, and ϵ is the tortuousity of Nuclepore, described below.

When compared to experimental data, the theory is usually presented in terms of an index of refraction $n = C_{\text{nonporous}}/C_{\text{porous}}$, where C_{porous} and $C_{\text{nonporous}}$ are the velocities on porous and nonporous (smooth) polycarbonate samples, respectively. For the case of unfilled pores, the quantities of interest in calculating the index of refraction are the extra fluid volume present due to the pore, ΔV, and the rate of change of that trapped volume

with changes in the flat surface film thickness h. The quantity ΔV and its derivative with respect to h can be determined if the relationship between h and the film thickness h' in the pore is established. This is done by equating the chemical potential μ_s of an atom at the surface of the flat film with that of an atom on the surface of the curved pore film μ_p. Neglecting terms common to both locations, the approximate potential balance is given by CGM as

$$\frac{\alpha}{h^3} = V(h',R) + \frac{\sigma}{\rho(R-h')} , \tag{15}$$

where α/h^3 is the van der Waals potential of an atom a distance h from the flat surface and $V(h',R)$ is the van der Waals potential for an atom a distance h' from the wall of a pore of radius R. CGM further approximate $V(h',R)$ as α/h'.[3] When the CGM theory is applied to index data in later sections, we will use the more accurate expression of Saam and Cole[5] given in Eq. (5).

If the pores are assumed to be perfect cylinders which are oriented at right angles to the surface, the CGM expression for the index in a case of unfilled pores can be written as $n^2 = 1 + \xi(\partial/\partial h)(\Delta V)$, where ξ is the areal density of pores. In an actual sample of Nuclepore, the pores are not precisely perpendicular to the surface, but instead vary from perpendicularity by an angle $0 \lesssim \theta \lesssim 34°$, as shown in Fig. 1. This effect is described in the calculation by defining a tortuosity[3] $\epsilon = \langle \sin^2\theta \rangle$ to account for the fact that a sound mode propagating down a pore can have a momentum component in the direction of the macroscopic mode propagating across the substrate. The index with the effect of tortuosity included is given by

$$n^2 = \left[1 + \xi \frac{\partial \Delta V}{\partial h}\right] \Big/ \left[1 + \epsilon \frac{\xi \Delta V}{2h}\right] . \tag{16}$$

When h is small, surface tension effects are minimal and h' is essentially equal to h. C_p is then simply C_3, and the index is a constant which depends only on the geometry of the sample:

$$n_0^2 \simeq (1 + A_p/2A_s)/(1 + \epsilon A_p/2A_s) , \tag{17}$$

where A_p is the surface area in the pores and A_s is the surface area of one face of the planar substrate, corrected for the presence of pore openings. As h increases, the approximation $h = h'$ is no longer valid; the surface tension due to the curvature of the film in a pore causes h' to become larger than h and the full expression for the index given in Eq. (16) must be used. As h' increases with increasing h, the restoring force for the film in the pore becomes weaker and $\partial(\Delta V)/\partial h$ grows, until a point is reached where the restoring force equals zero and the pore fills with helium (configuration III in Fig. 3).

When the pores are filled, $C_p = C_4$ and the expression for the index becomes

$$n^2 = \left[1 + \frac{C_3^2 V_p}{C_4^2 2h A_s}\right] \Big/ \left[1 + \frac{\epsilon V_p}{2h A_s}\right] \tag{18}$$

where V_p is the total fluid volume in the pores. Because C_4 is large compared to C_3 and because the volume of fluid V_p in the pores is much larger than the volume $2hA_s$ of film on the surfaces, this expression predicts an index less than unity for this regime. Intuitively, this fast mode is caused by the fact that the pores are not, on average, perpendicular to the direction of propagation of the third sound (that is, $\langle \sin^2\theta \rangle > 0$). Therefore, energy can be transmitted parallel to the surface through the pores as fourth sound more rapidly than it can propagate on the surface as third sound.

III. EXPERIMENTAL PROCEDURES AND RESULTS

A. Overview of experimental runs

The experiments were carried out in a conventional regulated pumped-bath dewar operated at temperatures from 1.4 to 1.8 K. Samples were sealed in a cylindrical brass chamber of volume of 435 cm^3. Except where otherwise noted, this chamber also housed a film reservoir of approximately 2 cm^2 each of 0.05 and 0.3 micron nominal diameter packed alumina powder to stabilize the film thickness. Because of our desire to make simultaneous third-sound and adsorption measurements, this apparatus did not have the ideal minimum dead volume typically used in adsorption measurements. However, our approach, which involves monitoring the adsorbed helium mass by a capacitance technique, avoids the negative effects of a large dead volume found in more usual adsorption measurements. Temperatures were measured with Allen-Bradley carbon resistors which were calibrated against the saturated vapor pressure,[17] P_0, of ^{4}He as measured by a MKS capacitance pressure gauge.[18]

The work described here represents the results of three separate but related experiments: a study of third-sound propagation on Nuclepore, capacitance measurements of the amount of condensed ^{4}He in the Nuclepore pores, and a simultaneous third-sound and capacitance experiment where third sound was propagated across a region of Nuclepore where simultaneous measurements of the pore capacitance were made.

Capacitor plates and third-sound drivers and detectors were deposited on the Nuclepore using standard evaporation techniques to apply $\simeq 500$ Å of Ag (capacitor plates), and ~ 200 Å each of Ag (third sound drivers) and Al (third sound bolometer detectors). More detailed discussion of individual substrate preparation will be given in the appropriate sections below. SEM photographs of Nuclepore samples taken before and after the metal evaporations show that the deposited material does not significantly change the pore opening diameter. The placement of the Ag and Al devices on the various substrates is shown in Fig. 4. Samples were mounted by clamping them to brass holders along opposite edges.

The thickness of the helium film in the experimental chamber was monitored in two ways. First, the MKS baratron pressure gauge was used to measure the pressure difference ΔP between the sample cell and either the main dewar helium reservoir or a small separate cell mounted 2 cm above the experimental cell, which was maintained at saturated vapor pressure P_0. The relationship between P and the thickness h is given[11] by

$$\frac{h^4}{\beta}+h^3=\alpha/[T\ln(P_0/P)] \tag{19}$$

where $P=P_0-\Delta P$ is the pressure in the experimental cell, β is the same retardation term as in Eq. (1), and the van der Waals constant α is used with units of (layers^3) K for h and β in atomic layers. The second method used to determine the film thickness involved the measurement of the third sound velocity on glass. The thickness is calculated using Eq. (2), with[12] D (glass)$=0.5+1.13\ T\ \rho/\rho_s$ as described in the discussion relevant to Eq. (2). Since the film thickness values deduced from a given P and P_0 or from the measured third sound velocity depend on the values of α and β for a particular substrate, the film thicknesses reported will be for glass, where the values $\alpha_g=27$ (layers)^3 K and $\beta_g=41.7$ layers are known.[11] The film thickness values deduced separately from the pressure measurements and the measurements of the velocity of third sound agree well at thinner coverages; at higher coverages ($h\gtrsim 15$ layers), ΔP is very small compared to P_0 and small errors in measuring ΔP can cause large errors in the film thickness calculated from the pressure measurements. Because of this, the film thicknesses reported here have been calculated from measured third sound velocities [Eq. (2)] on glass wherever possible. In a few instances, the reference third sound substrate was clean Nuclepore instead of glass; for these runs, the measured index of refraction between glass and clean Nuclepore (described in the next section) was used to deduce the equivalent glass velocity.

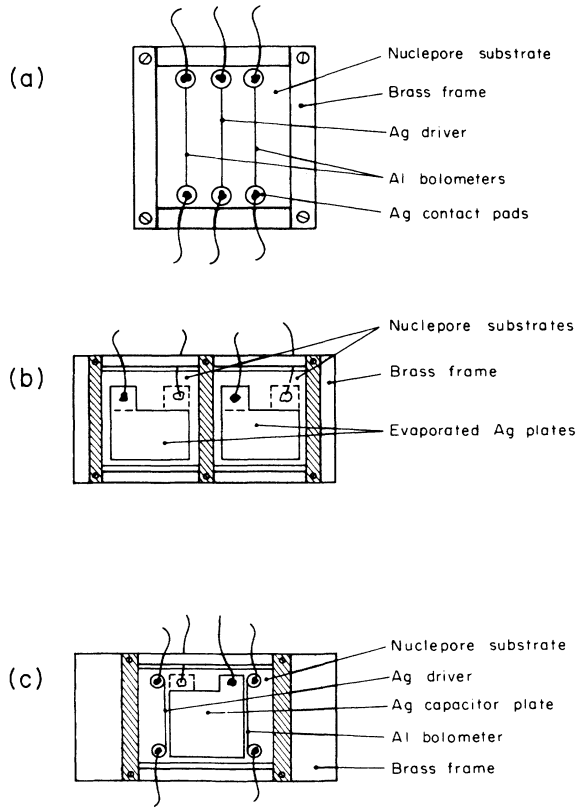

FIG. 4. (a) Typical third-sound time-of-flight substrate configuration for both porous and nonporous samples. The center strip is an Ag driver with Al bolometers located 0.635 cm away on either side. Total sample dimensions are 2.54 cm (between clamps)$\times$2.86 cm. Typically only one detector was used. Cu wires (No. 40) were attached to the Ag pads with Silver Print (Ref. 20). Glass third sound time-of-flight substrates used an identical strip geometry, but the glass was held loosely rather than clamped. (b) Nuclepore capacitors used for the capacitance studies. Ag plates with overlapping plate dimensions 1.0×1.5 cm^2 and an approximate thickness of 500 Å were evaporated on opposite Nuclepore surfaces. In addition, each plate had a 0.5×0.5 cm^2 extension to which No. 40 Cu wires were attached, again using Silver Print. (c) Device configuration for the simultaneous third-sound and/or capacitance measurements. Capacitor plate dimensions (excluding tabs) are 1.27×1.43 cm^2. The spacing between the capacitor plate and the driver or bolometer is 0.08 cm. The substrate shown is porous Nuclepore. The configuration for the nonporous substrate is identical except that it does not have a capacitor plate on the back side.

B. Third sound time-of-flight studies

Third sound measurements on Nuclepore with nominal pore diameters of 800 Å and 2000 Å, and measurements on nonporous (smooth) Nuclepore and glass have been made using traditional pulsed third sound time-of-flight (TOF) techniques.[19] Nuclepore samples with approximate dimensions 2 cm$\times$4 cm were prepared by evaporating third sound drivers (Ag) and detectors (Al) with dimensions 150 microns$\times$1.5 cm which are separated by 0.635 cm, as shown in Fig. 4(a). Strip resistances were typically 300 to 700 Ω at room temperature. Evaporated Ag pads facilitated electrical contact to the strips; Ag paint[20] was used to fasten No. 40 Cu wires to the pads.

Voltage pulses (single cycle, zero offset, clamped sine) with equivalent frequencies in the range 1 to 50 kHz were applied to the drivers at a pulse rate of $\sim$20 Hz and with a typical integrated energy per pulse of 0.1–10 nJ. The resulting third sound pulses were detected by the Al bolometers, which were biased at their superconducting transition using currents typically in the range 50–200 μA. Varying the bias current and the applied magnetic field (0–100 G) allowed for the tuning of the bolometers' transition temperatures from 1.4 to 1.8 K. Typical bolometer sensitivities were 1000–5000 Ω/K. The time of flight τ of a third sound pulse was defined to be the time between the generation of the peak of the drive pulse and the arrival of the point of maximum amplitude of a third-sound pulse at the detector. The corresponding third-sound velocity was taken to be the macroscopic distance between the driver and detector divided by τ. Signal averaging techniques[21] were used to improve the signal-to-noise ratio of the detected third-sound signals.

Three different pairs of TOF samples were studied. First, third sound times of flight were measured simultaneously on the smooth (nonporous) Nuclepore sample (τ_s) and on a standard borosilicate microscope slide (τ_g) to determine the "smoothness' of the smooth Nuclepore relative to glass. The index of refraction of the system, defined in the traditional way as $n=\tau_s/\tau_g$, is shown in Fig. 5 as a function of ^{4}He film thickness on glass. The rise in n for increasing h is reminiscent of earlier observa-

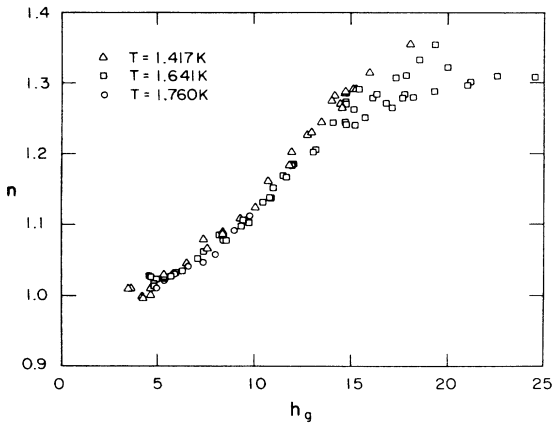

FIG. 5. Observed index of refraction, $n=\tau_s/\tau_g$, for the case of smooth Nuclepore and glass as a function of the helium film thickness h_g on glass for $T=1.417$, 1.641, and 1.760 K. The rise in index at thicker coverages suggests a weak, long-length-scale roughness to the smooth Nuclepore substrate. h_g was determined from third sound velocity on glass using Eq. (2).

tions[22] and indicates that there is some long-length-scale roughness on the smooth Nuclepore which traps extra ^{4}He at higher film coverages. Weak hysteresis is observed at higher coverages. The data shown is for 1.41, 1.64, and 1.76 K.

This same data can be used to determine the parameter D for Nuclepore, as described in Sec. II B, by rewriting the simple velocity equation [Eq. (3)] using $h_N=h_g(\alpha_N/\alpha_g)^{1/3}$, with $\alpha_g=27$ layers^3 K:

$$\Gamma=\frac{C_3^2h_g^4}{(\rho_s/\rho)3\alpha_g(1+TS/L)^2}=h_g-D(\alpha_g/\alpha_N)^{1/3}\ , \qquad (20)$$

where α_N is the van der Waals constant for Nuclepore. A plot of Γ as a function of h_g for the smooth Nuclepore sample is shown in Fig. 6, with the intercepts $D(27/\alpha_N)^{1/3}$ for the three temperatures given in Table II. The temperature dependence of D measured for smooth

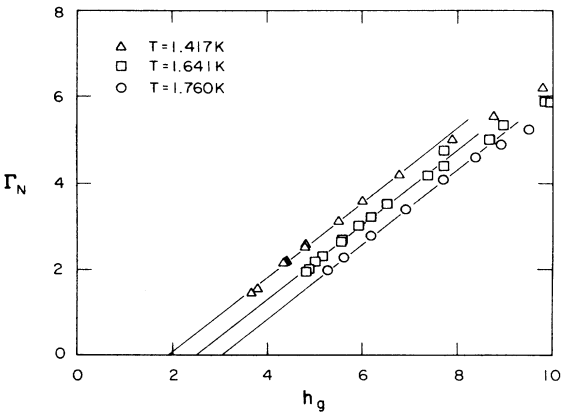

FIG. 6. Determination of the parameter D for polycarbonate Nuclepore substrate material. Here $\Gamma=C_3^2h_g^4/(\rho_s/\rho)3\alpha_g[1+TS/L]^2$. Intercept values $D(\alpha_g/\alpha_N)^{1/3}$ are given in Table II.

TABLE II. Nuclepore D parameter for three temperatures.

Temperature (K)	$D[(\alpha_g=27)/\alpha_N]^{1/3}$ (layers)	$D(\alpha_N=50$ layers K) (layers)
1.417	1.93	2.37
1.641	2.55	3.13
1.760	3.08	3.78

Nuclepore is consistent with that for glass; that is

$$D=A+BT/(\rho_s/\rho)\ , \qquad (21)$$

where A and B are constants. For glass,[12] $A=0.5$ and $B=1.13$; for smooth Nuclepore we find $A=-0.25$ and $B=1.64$. These values for Nuclepore are clearly unphysical at very low temperatures and should be taken as representative of the data only over the limited temperature range studied.

The second pair of (TOF) samples studied consisted of the smooth Nuclepore sample from the run just described and a porous sample with 2000-Å diameter pores,[1] prepared using techniques identical to those used for the earlier TOF samples. The index of refraction $n=\tau_{\text{porous}}/\tau_s$ between the two substrates is shown as a function of h_g in Fig. 7, with arrows denoting the direction in which the data was taken. No glass time of flight was available for this run; the film thickness was determined from the time of flight on the smooth Nuclepore using the measured index of refraction between smooth Nuclepore and glass (Fig. 5) and Eq. (2). At thinner coverages, the index between 2000 Å and smooth Nuclepore shows a plateau at $n=2.7$ which is essentially independent of thickness. As the thickness increases, however, the index begins to rise, then drops abruptly to $n\approx\frac{1}{4}$ as the pores condense, and remains essentially constant from there out to the highest coverages studied. This behavior

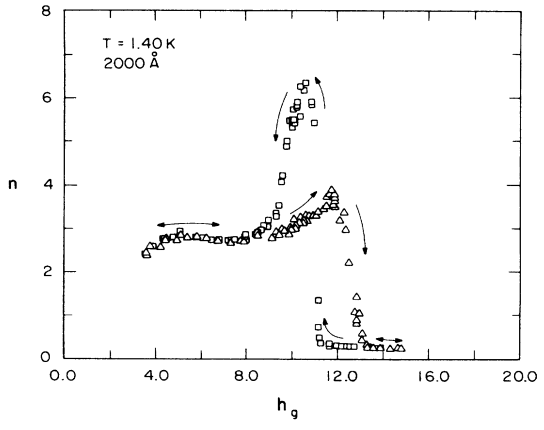

FIG. 7. Observed index of refraction, $n=\tau_p/\tau_s$, for the case of 2000-Å and smooth Nuclepore as a function of the helium film thickness on glass at 1.40 K. Arrows indicate the direction in which the data were taken, i.e., triangles (squares) denote data taken while increasing (decreasing) the film thickness. These data have been previously reported (Ref. 2).

is explained by the CGM theory for the index described in Sec. II D. In the low coverage plateau region, the film thickness in the pores is essentially equal to the thickness on the surface and the index depends only on the ratio of pore surface area to flat surface area. The turn down of the index at the lowest coverages is the result of the Kosterlitz-Thouless transition on the relevant substrates; this effect will be discussed in somewhat more detail in Sec. III E. As the pores come closer to condensation, dh/dh' and the index increase until the pores condense and the fast mode appears. This part of the index curve was originally analyzed[2] by assuming that all of the pores had the same radius. For this case, CGM predict that n will diverge at the value of h where the pores condense. In the physical system, a distribution of pore radii, combined with the inability of a pore to be infinitesimally close to condensation without being condensed by small fluctuations in film height in the pore, act to smooth the transition from the slow mode ($n>1$) to the fast mode ($n<1$). A quantitative discussion of both of these effects follows in Sec. III D. If the film is thinned, beginning at a coverage where the pores are completely condensed, the index does not retrace the filling curve. Instead, it remains low to coverages smaller than that at which the pores filled, then jumps very abruptly to a value close to 6. Thinning the film further causes the index to decrease and ultimately to come into line with the fill data in the region of the low-coverage plateau. This hysteretic behavior is expected on the basis of the calculations of both SC and CGM. A quantitative prediction for the detailed behavior of the index as the pores empty was not made by CGM because the configuration of the film in this regime is apparently complex. It is believed that when the index is near its maximum value the film is in a configuration similar to II in Fig. 3. The simultaneous TOF and capacitance studies described below were undertaken in part to learn more about the film configuration in this regime.

The third pair of TOF samples consisted of the same smooth Nuclepore sample used above and a 800-Å TOF substrate. The index of refraction for this system is shown in Fig. 8. The features of the plot are essentially the same as those for the 2000-Å Nuclepore, but have been shifted to lower film thickness, as might be expected for a smaller pore size. As with the 2000-Å run, the film thickness h_g was calculated from the smooth Nuclepore time of flight. In order to learn something about how the fractional filling of the disordered array of pores in Nuclepore affects the frequency dependence of third sound attenuation, a study was done of the ratio of amplitudes A, $R = A_{\text{porous}}/A_{\text{smooth}}$ of the received sound pulses on the porous and smooth substrates as a function of the frequency (1/width) of the drive pulse for several locations on the index curve. The locations are marked with the letters $A-G$ in Fig. 8, and the ratio R, normalized to 1.0 at 2 kHz, is shown in Fig. 9. The most dramatic attenuation of higher (10 kHz) frequencies occurs at G, the peak of the index curve for emptying pores.

C. Capacitance studies

The next experiment was motivated by a desire to better understand the hysteresis observed in third-sound data on Nuclepore. The amount of helium adsorbed in Nuclepore filters was measured using a capacitive technique. Due to the changing amount of dielectric present, the measured capacitance changes as the helium film thickness inside the pores changes. Silver capacitor plates with an area of 1.53 cm^2 were evaporated directly onto each side of a Nuclepore filter, as shown in Fig. 4(b), with copper wire leads attached using silver paint. The capacitance was measured using a General Radio 1615-A capacitance bridge; the capacitors were driven with a 100-mV

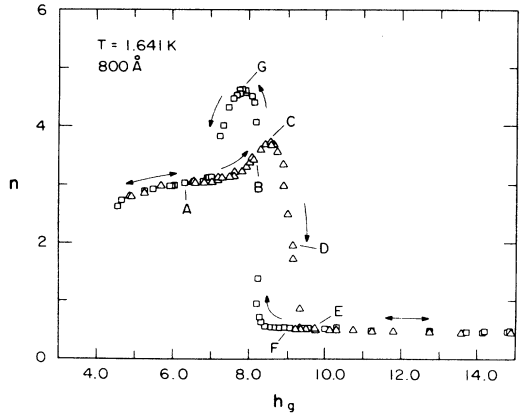

FIG. 8. Observed index of refraction, $n=\tau_p/\tau_s$, for the case of 800-Å and smooth Nuclepore as a function of the helium film thickness on glass at 1.641 K. As in Fig. 7, arrows indicate the direction in which the data were taken. The index for the 800-Å Nuclepore is qualitatively very similar to the index for the 2000-Å sample, but the features are shifted to thinner coverages in the 800-Å data. Positions on the curve labeled with letters indicate the locations where the data displayed in Fig. 9 were taken.

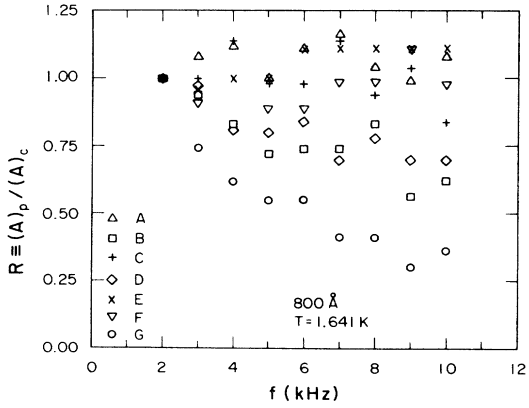

FIG. 9. Ratio of the received third-sound amplitudes on the 800-Å and smooth Nuclepore as a function of the frequency (1/width) of the drive pulses for locations on the index curve labeled in Fig. 8. The most pronounced attenuation of higher frequencies occurs at the peak of the index curve as the pores are emptied.

peak-to-peak sine wave at 293 Hz. Typical power dissipated in the capacitors was ~ 1 nW. We found that a capacitance measurement taken with the drive to the capacitor applied continuously did not differ from a measurement taken immediately after reconnecting the drive following a 10-min period when the drive was not applied. We conclude that the small amount of power dissipated did not affect the measurement. A glass third sound TOF substrate was also prepared in the manner described earlier. In this experiment, the capacitance of helium in the pores of 800 and 2000 Å Nuclepore was measured simultaneously with measurements of the time of flight on glass for two temperatures, $T=1.641$ and 1.417K. It was found that adding gas to the experimental cell too fast would cause the pores to fill prematurely. This was remedied by introducing gas continuously through 0.5 m of capillary with an experimentally determined effective inner radius of 0.043 cm by applying a pressure difference of the order of 25 Torr across the capillary. Using this method, the film thickness on glass increased at a rate of roughly 0.006 atomic layers/min. Figure 10(a) shows the capacitance of the 2000-Å sample, reported as $\Delta C/C_{\rm full}=(C-C_{\rm full})/C_{\rm full}$, as a function of h_g for $T=1.64$ K. $C_{\rm full}$ is the value of capacitance when the pores are fully condensed; for the 2000-Å sample at $T=1.641$ K, $C_{\rm full}=316.138\pm0.002$ pF. Figure 10(b) shows data taken at $T=1.641$ for the 800-Å sample, for which $C_{\rm full}=587.827\pm0.002$ pF. The data taken at $T=1.417$ K was similar to that at 1.64 K for both samples. The film thickness on glass is determined from the the third-sound velocity on glass, as discussed in Sec. II B. By examining the linear rise in capacitance in the thin film region, the change in capacitance per layer of film in the pore may be determined. Using the approximation that $D_N=D_g(\alpha_N/\alpha_g)^{1/3}$ for thin films, with $\alpha_N=50$ (layer)^{3}K and $\alpha_g=27$ (layer)^{3}K, the sensitivities of the capacitors were found to be 0.0202 pf/layer and 0.0345 pf/layer for the 2000- and 800-Å Nuclepore, respectively.

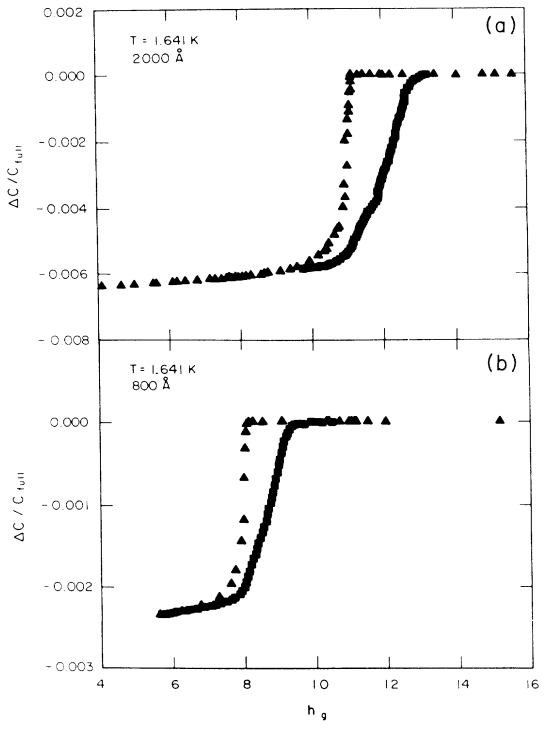

FIG. 10. (a) Capacitance C, reported as $(C-C_{\rm full})/C_{\rm full}$, as a function of film thickness on glass for the 2000-Å-diameter Nuclepore at $T=1.641$. (b) $(C-C_{\rm full})/C_{\rm full}$ as a function of film thickness on glass for the 800-Å Nuclepore at $T=1.641$. Squares denote adsorption and triangles denote desorption.

Hysteresis as a function of film thickness is evident; this is consistent with the third-sound index data. It is clear, however, that the pores do not fill at constant pressure, or constant thickness, as is predicted by Saam and Cole[5] for pores with a single radius, although for the 2000-Å (and the 800-Å to a lesser extent) Nuclepore, the pores appear to initially empty at a constant pressure. There are two possible explanations for the non-ideal character of the curves. A distribution in pore sizes would smear out the hysteresis loop, since the different size pores would have different critical and metastable radii. This possibility will be discussed in detail later. The pores are also non-ideal in that they are not perfect cylinders, are not perfectly parallel, and intersect; each factor would tend to smear out the adsorption curves. Fits to the capacitance data using the theory of Saam and Cole[5] will be discussed in the next section.

D. Simultaneous third sound and capacitance

The next experiment directly related the third-sound time of flight and the amount of helium adsorbed as measured by the capacitive technique. Capacitor plates were deposited onto 2000-Å pore-diameter Nuclepore and a third sound driver and detector were evaporated on either side of the plate with the geometry shown in Fig. 4(c). The capacitor plates were 1.27 cm$\times$1.43 cm, with the third sound being propagated across the longer dimension; the driver and detector were separated by 1.48 cm, so that almost the entire third sound path was across the capacitor plate. A sample of nonporous Nuclepore was also prepared with a driver and detector and a silver plate between the two, in exactly the same geometry as the porous sample. On the nonporous sample, however, the silver plate was not used as part of a capacitor, but was included so that the surface over which third sound propagated would be as similar as possible for the two substrates. The evaporations were performed as described earlier.

We simultaneously measured third-sound times of flight on the porous and the non-porous substrate and capacitance for the porous substrate as a function of h at $T=1.64$ K. In one set of experimental runs the film reservoir was the packed powder described earlier; in a separate run the reservoir was 15 sheets of 2000-Å Nuclepore which were 9 cm in diameter. For the first run, with the powder reservoir, the value of the capacitance with the pores filled was 393.478 ± 0.001 pF at $T=1.641$ K. After cycling to room temperature to change the reservoir to Nuclepore filters, the full capacitance value shifted to 394.737 pF, most probably because the leads

were disturbed. The last run of this simultaneous third sound and capacitance data set included a glass time-of-flight substrate, enabling us to establish the relation between velocity on the nonporous Nuclepore and film thickness on glass. Gas was added in discrete amounts through a capillary, as described in the preceding section. As in the capacitance runs, slow, careful addition of gas was necessary to avoid prematurely filling the pores.

The data for the index of refraction between the porous and non-porous Nuclepore and the capacitance data are shown in Figs. 11(a) and 11(b), respectively, as a function of film thickness on glass. These data appear more complicated than those shown previously in Figs. 7 and 10, because in addition to the study of hysteresis, in some runs ^{4}He was withdrawn prior to competely filling the pores, shown with $+$'s, or ^{4}He was added before the pores had been emptied to the point where the desorption curve meets the adsorption curve, shown with $\times$'s. (It should be pointed out that the index data obtained in the early TOF run (Fig. 7) differ noticeably from those obtained in the simultaneous TOF capacitance run [Fig. 11(a)], particularly in the location of the peak in the adsorption curve, even though the samples came from the same batch. Because the evaporation of the silver capacitor plates did not significantly change the pore opening diameters, it is most probable that this difference is the result of changing to the use of the very small capillary described in the previous section to add gas to the sample cell. In the early TOF runs, gas was added more quickly.) There is a slight inflection in the capacitance curve at point A which corresponds to the peak of the index during adsorption, also labeled point A. At point B the pores are fully condensed, as is evident from both the index and capacitance curves, and at point C both curves show the pores just beginning to empty during desorption. If the assumption is made that the sensitivity of the capacitor to helium is independent of the amount of helium in the pores, then a fractional change in capacitance corresponds directly to the same fractional change in the mass of helium in the pores. The index is plotted as a function of $\Delta C/C_{\text{full}}$ in Fig. 12, and points A, B, and C are labeled as described in Fig. 11. It is clear that the same value of $\Delta C/C_{\text{full}}$, or the same mass of helium adsorbed, can correspond to two very different values of the index. The higher value of n corresponds to configuration II from Fig. 3 during desorption, and the lower value of n corresponds to configuration I from the same figure during adsorption. This type of plot is a good confirmation of the prediction that there can be two very different configurations for the liquid in the pore for a given mass of ^{4}He adsorbed.

Calculations were performed to compare the index data and capacitance data to the theories of CGM (Sec. II D) and SC (Sec. II D), respectively. It was found that modeling the substrate using pores of a single radius would not produce good fits to either the index or the capacitance data; the breadth of the transition of unfilled to filled

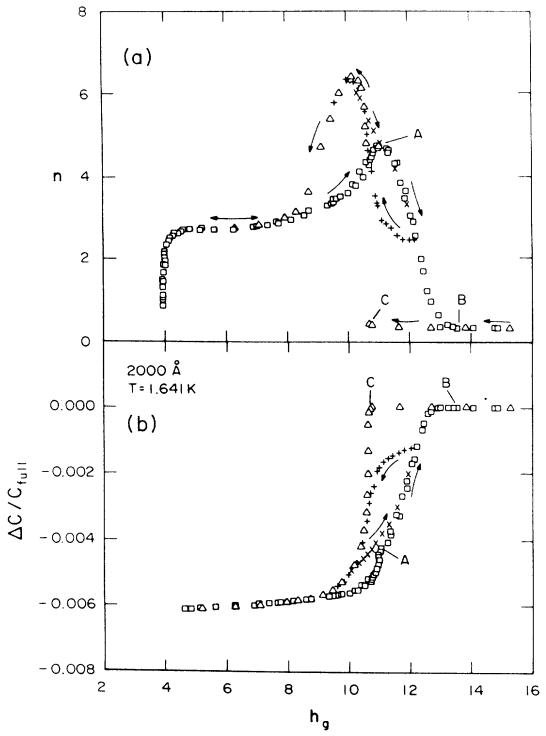

FIG. 11. (a) Observed index of refraction $n=\tau_p/\tau_s$ for the simultaneous third-sound and/or capacitance Nuclepore substrate. Squares denote adsorption and triangles denote desorption. In addition, data denoted by "$+$" were taken by decreasing the flat surface film thickness before the pores had completely condensed on an adsorption run. Similarly, data denoted by "$\times$" were taken by increasing the flat surface film thickness from the middle of a desorption run. Points labeled A, B, and C match those with the same labels in figure (b) and are included to emphasize the alignment of key features in the two graphs. (b) Observed capacitance $\Delta C/C_{\text{full}}=(C-C_{\text{full}})/C_{\text{full}}$ for the simultaneous third sound/capacitance substrate. The symbols denoting data are the same as in (a).

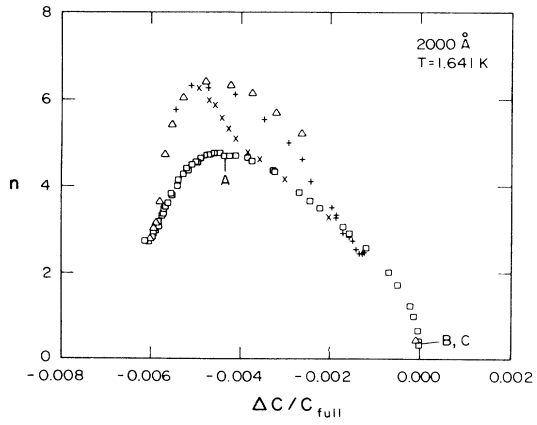

FIG. 12. Index of refraction for a 2000-Å Nuclepore as a function of $(C-C_{\text{full}})/C_{\text{full}}$. The labels A, B, and C, and the symbols denoting data, are the same as in Fig. 11. Note that there is a range of values of $(C-C_{\text{full}})/C_{\text{full}}$ for which a given value of $(C-C_{\text{full}})/C_{\text{full}}$ (and therefore a given amount of He in the pores) can result in two very different values of the index. This implies that in the hysteretic region there is more than one stable configuration for a given number of ^{4}He atoms.

pores cannot be explained if all of the pores have the same radius. The calculation of the index of refraction as a function of the film thickness on glass using the theory of CGM was straightforward; some pore distribution was chosen and the index was calculated for a given value of h_g by seeing what fraction of the pores are condensed at that value of h_g and adding the contributions of the condensed and uncondensed pores independently. It was found that a very high value of the index ($n > 10$) resulted if even a very small fraction of the pores were allowed to come arbitrarily close to condensation. In a real system, effects such as vibration and fluctuations of the film thickness due to the addition of gas to the sample cell prevent pores from remaining arbitrarily close to condensation. To include this effect in the calculation, we introduced a parameter δ, which was defined as follows. At each value of the film thickness h_g on glass, we looked at the pore distribution and determined, using the CGM theory, not only which pores had condensed, but also which pores would condense if h_g were to be increased by an amount δ. These additional pores were then also taken to be condensed when calculating n at the original value of h_g. The parameters used as input for the index calculation were those determining the pore distribution plus the tortuosity ϵ, the number of pores per cm^2 ξ, and δ. The solid line in Fig. 13 shows the agreement obtained with the index data for the values $\xi = 3.8 \times 10^8/\text{cm}^2$, $\epsilon = 0.07$, $\delta = 0.8$ layers, and the pore distribution shown in Fig. 14, which has the form $s(R) = \exp\{-[(920-R)/50]^2\}$ for $R < 920$ Å and $s(R) = 2\exp\{-2[(R-920)/250]^4\}$ for $R > 920$ Å. The dotted curve in Fig. 13 is the index calculated by using the pore distribution which gave agreement with the capacitance data (Fig. 16, discussed below).

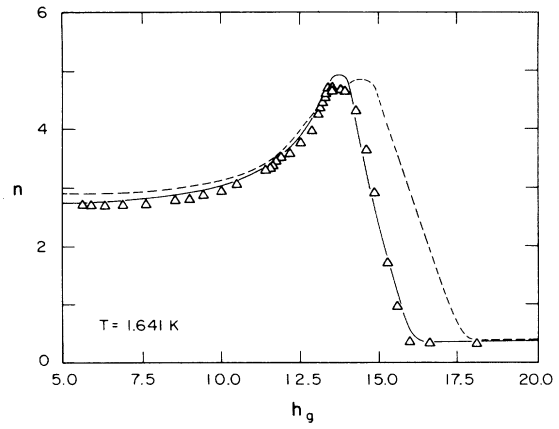

FIG. 13. Adsorption data from Fig. 11(a). Shown with the results of two calculations using the Cohen-Guyer-Machta theory for third sound on Nuclepore. The dashed curve is the index of refraction predicted by the CMG theory using the pore distribution [Fig. 16(a)] which best fits the 2000-Å adsorption capacitance data. The solid curve is the index of refraction predicted by the CMG theory for a pore distribution, shown in Fig. 14, which has been chosen specifically to optimize agreement with the index data.

In order to compare the capacitance data to SC theory, it was necessary to measure the capacitance with completely empty pores; this was done by pumping on the cell with a leak detector at room temperature, cooling to the temperature of interest, and then measuring the capacitance, called C_e. The experimental quantity $\%C = (C - C_e)/(C_{\text{full}} - C_e)$ can then be compared to the predicted filling fraction $X = 1 - Y^2$ of SC, if one again makes the assumption that the sensitivity of the capacitor is independent of the amount of helium adsorbed. We make this comparison later.

The capacitance of the Nuclepore with no helium in the cell was 392.190 pf for the 2000-Å sample used in the simultaneous TOF and capacitance studies with a Nuclepore reservoir. This empty value of capacitance was found to vary linearly with temperature from a value of 392.155 pf at 1.473 K to 392.209 pf at 1.736 K. For this capacitor, the total change in capacitance between full and empty pores was found to be 2.547 ± 0.01 pf at $T = 1.641$ K; this value did not change after cycling to room temperature.

Separate sets of data were taken using different capacitors evaporated onto 2000- and 800-Å Nuclepore. The geometry of these capacitors was the same as that described in Sec. III C. The glass time of flight substrate was included, but no Nuclepore time of flight was present for this set of data. This data run had a film reservoir consisting of 7 cm^3 of 0.05-μm diam. packed alumina powder (compared to 2 cm^3 each of 0.3 and 0.05-μm diam. previously). The empty value of capacitance was 587.500 ± 0.002 pf for the 800-Å Nuclepore, and 316.145 ± 0.003 pf for the 2000-Å case; the full values were 589.010 ± 0.002 and 318.138 ± 0.002 pf, respectively.

We carried out a calculation which determines the pore radius from the total change in capacitance. This calculation assumes the pores are perfect, nonintersecting cylinders, that the electric potential is uniform across the surface of the capacitor plate, and that the ^{4}He liquid ap-

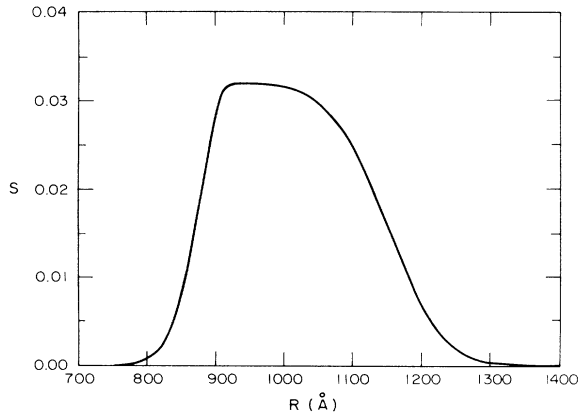

FIG. 14. Distribution of pore radii which gives the solid curve of Fig. 13.

pears as a dielectric added in parallel with the Nuclepore. The change in capacitance is due to the difference in dielectric constant between vacuum and ^{4}He liquid. The total change in capacitance for the capacitors described in the preceding paragraph is 1.993 and 1.510 pf for the 2000- and the 800-Å Nuclepores, respectively. Using $\xi = 4 \times 10^8/\text{cm}^2$ and $\epsilon - 1 = 0.055$ (where ϵ is the dielectric constant of ^{4}He) gives pore *radii* of 1459 and 984 Å for 2000- and 800-Å diameter Nuclepores, respectively; this radius for the 2000-Å Nuclepore is consistent with the work of Chen and co-workers.[6] This simple calculation does not consider how the electric field lines are altered by the presence of the pores in the Nuclepore. Given this, the validity of the pore radius calculated above is questionable; a more detailed calculation is necessary.

The data is shown in Figs. 15(a) and 15(b), where $\%C$ is shown as a function of P/P_0 for each porous sample, along with calculated curves for the filling fraction obtained from pore distributions to be discussed later. For the 2000-Å Nuclepore, the earlier data taken with a Nuclepore reservoir and simultaneous TOF on Nuclepore shows very similar behavior. It is evident from our various studies that the type of film reservoir present does not affect the adsorption isotherm. It was thought earlier that the size of the film reservoir present might affect the steepness of the adsorption curves; a reservoir which was too small might artificially broaden the curves if not enough atoms were present to condense the pores completely when the film reached the critical thickness. Since no significant difference is seen between the 2000-Å adsorption curve with a Nuclepore reservoir and the curve with a large packed powder reservoir, the fact that the pores do not fill at constant pressure is not due to an insufficient reservoir of helium atoms.

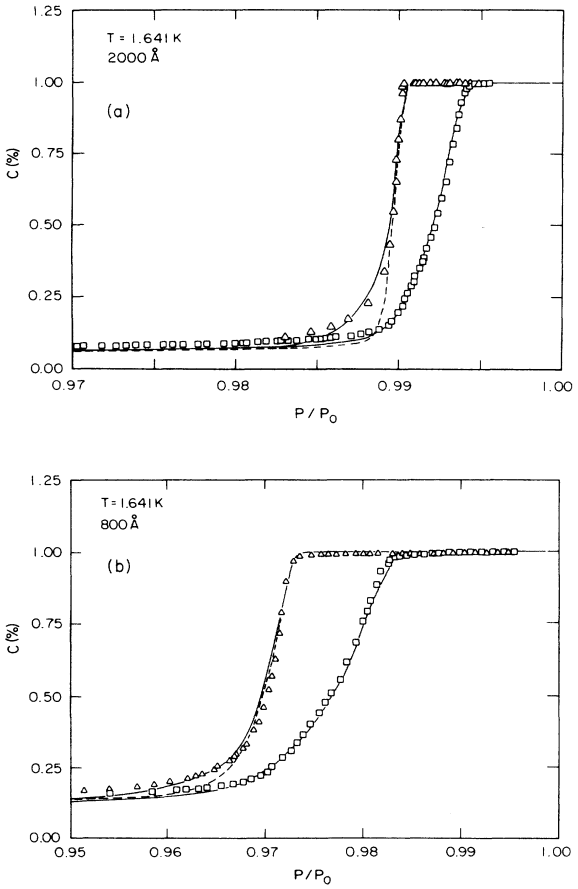

FIG. 15. Capacitance C, given as $\%C = (C - C_E)/(C_{\text{full}} - C_e)$, as a function of reduced pressure P/P_0 for the 2000-Å-diameter Nuclepore (a) and 800-Å Nuclepore (b) at $T = 1.641$ K. The squares denote adsorption, the triangles denote desorption, and the solid lines are calculations using the theory of Saam and Cole and distributions of pore radii shown in Fig. 16. The dashed lines show alternate calculations, as discussed in the text.

We use the theory of Saam and Cole with a distribution in pore radii to compare the adsorption and desorption data to theory. The adsorption or desorption isotherm for a distribution is found by averaging the contributions from the different pore sizes, taking into account that P_c and P_m are different for each pore size. The manufacturers' specifications for the pore openings led us to start with a skewed Gaussian distribution which was broad on the small pore side of the distribution, and sharp for large pores. It was found that a single distribution would not agree with both the adsorption and the desorption curves. This is perhaps understandable if the openings of the pores have a sharper distribution than the interiors of the pores, and control the desorption.

The calculations shown in Fig. 15 use the theory of SC with different distributions in pore radii for adsorption and desorption. For the adsorption isotherm, a value of δ equal to that found from the index calculations is used. The optimal calculations, shown with solid lines in Fig. 15, use the distributions shown in Fig. 16 with the solid lines; the form of the distribution for the 2000-Å adsorption is

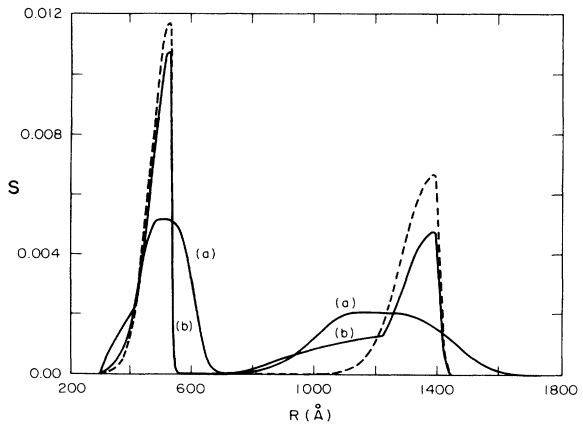

FIG. 16. (a) Distribution of pore radii used for the capacitance adsorption calculations in Fig. 15. (b) Distribution of pore radii for desorption calculations in Fig. 15. The exact forms of the distributions are described in the text, with the solid lines showing the best agreement, and the dashed lines giving alternate calculations for the desorption data.

$s(R)=\exp\{-[(1135-R)/150]^2\}$, $R \leq 1135$ Å

$s(R)=2\exp\{-2[(R-1135)/350]^4\}$, $R > 1135$ Å

while the optimal distribution for the 2000-Å desorption is

$s(R)=\exp\{-[(1390-R)/900]^2\}-C$, $R < 1225$ Å

$s(R)=\exp\{-[(1390-R)/120]^2\}$, $1225 \leq R \leq 1390$ Å

$s(R)=\exp\{-[(R-1390)/20]^2\}$, $R > 1390$ Å

where R is the pore radius in angstroms, and C is a constant which ensures that the distribution is continuous. The above form of the pore distribution for the desorption curve was necessary to fit the data. For comparison, the result of a pore distribution with $s(R)=\exp\{-[(1390-R)/120]^2\}$ for $R<1390$ Å and $s(R)=\exp\{-[(1390-R)/20]^2\}$, for $R>1390$ Å is shown in Fig. 15(a) with a dashed line. The corresponding pore distribution is shown in Fig. 16 with a dashed line. This type of distribution does not fit the desorption data as well as does the distribution shown with the solid lines. The optimal distribution for the 800-Å adsorption is

$s(R)=\exp\{-[(490-R)/70]^2\}$, $R \leq 490$ Å

$s(R)=2\exp\{-2[(490-R)/130]^4\}$, $R > 490$ Å

and the optimal distribution for the 800-Å desorption is

$s(R)=\exp\{-[(525-R)/325]^2\}$, $R < 420$ Å

$s(R)=\exp\{-[(525-R)/70]^2\}$, $420 \leq R \leq 525$ Å

$s(R)=\exp\{-[(525-R)/10]^2\}$, $R > 525$ Å .

It was also found that good agreement to the 800-Å desorption curve could not be obtained with a simpler two function pore-distribution; such a calculation is shown in Fig. 15(b) and in Fig. 16 with dashed lines. A van der Waals constant of $\alpha_N = 50$ (layers)^3 K was used in these calculations; the results, however, are not particularly sensitive to α_N. Using $\alpha_N = 35$ (layers)^3 K gives an optimal pore distribution which differs from those given above by only a 1.7% shift in the position of the peak of the distribution. To determine the effect of δ on adsorption curves, calculations with $\delta=0$ were performed. Using $\delta=0$ caused the optimal pore distributions for adsorption to be shifted to the left (to lower radius values) by 236 and 122 Å for the 2000- and 800-Å-diameter Nuclepore, respectively. This would place the mean radius of the adsorption distribution below the mean radius of the desorption distribution. One would expect a much broader desorption curve than we observe if the pore openings were larger than the interior of the pore. If one considers that the adsorption is most likely governed by the interior of the pore, while the desorption is governed by the pore openings, it seems unlikely that the interior of the pore is smaller than the opening.

E. Kosterlitz-Thouless data

A liquid ^{4}He film is an example of a system which undergoes a Kosterlitz-Thouless[4,23] phase transition in two dimensions. The theory of Kosterlitz and Thouless examines the role of quantized vorticity in the film, and gives an explanation of the superfluid transition based on the behavior of the vortices. Above the transition temperature T_c the vortices are free to move about; below T_c single vortices are bound into pairs of zero net vorticity. The most striking prediction of the theory is the prediction of a universal jump in the areal superfluid density at the onset temperature T_c. The superfluid areal density σ_s is predicted to jump from zero above T_c to a finite value at T_c, given by

$$\sigma_s(T_c)/T_c = 3.49\times10^{-9}\ \text{g/cm}^2\ \text{K} . \quad (22)$$

Third sound is sensitive to the superfluid density, as can be seen in Eq. (2), and can be used as a probe of the superfluid transition. Relevant to the work we have done here, on a flat substrate, as a function of film thickness at fixed temperature, third sound is observed to disappear[24–26] below a temperature-dependent critical thickness D_c; in the static theory the disappearance of third sound is interpreted to be due to a discontinuous jump in σ_s.

The theory of Kosterlitz and Thouless[4] has been extended by Ambegaokar *et al.*[27] (AHNS) to include the effects of the finite frequencies and finite flow velocities encountered in experiments designed to study the superfluid transition; the propagation of third sound and the torsional oscillator are two such experimental techniques. AHNS theory calculates the effect of the diffusive motion of the vortices and predicts that the transition will be broadened and be accompanied by a peak in the dissipation of (for example) the torsional oscillator signal or a maximum in the third sound attenuation. The broadened transition and the associated peak in attenuation have been seen in helium films adsorbed on flat substrates,[28] in good agreement with AHNS theory.

Experiments with helium films adsorbed on porous substrates, however, show that the transition is altered from the flat substrate case. The work of Kotsubo and Williams on Al_2O_3 packed powders[29] shows a broadened transition in which the superfluid density goes continuously to zero, in contrast to the abrupt jump of the flat substrate transition. In addition, these experiments show no sharp peak in the dissipation, also in contrast to the flat substrate case. Kotsubo and Williams have developed a theory in which the finite size and curvature of the powder grains on which the helium is adsorbed are responsible for the broadening of the transition and the observed attenuation in their Al_2O_3 third-sound studies. In view of this it seemed appropriate to examine the superfluid transition on Nuclepore and compare it to the transition on a smooth substrate of the same material.

A plot of third sound velocity versus film thickness for porous and nonporous Nuclepore is shown in Fig. 17. The film thickness on the nonporous Nuclepore is determined from Eq. (19); for the porous Nuclepore, the film thickness inside the pore is determined using Eq. (9). A van der Waals constant of $\alpha_N = 50$ (layers)^3 K is used. A pore radius of 1025 Å was used in Eq. (9); for these very thin films, however, using a pore radius as large as 1500 Å caused a negligible change. Given the very thin film, the cubic approximation to the van der Waals potential in

the pore is used here rather than the hypergeometric function of SC, and retardation effects are neglected. Neglecting retardation is equivalent to setting $\beta=\infty$ in Eq. (19). We found that as the film thickness became thinner, the third-sound pulse on the porous substrate was sharper than that on the nonporous substrate, and that for film thicknesses at which the pulse had disappeared on the nonporous substrate, a pulse was still visible on the porous substrate. The peak in the velocity occurs at a thinner flat surface film thickness for the porous substrate than for the nonporous substrate. This is perhaps expected since the film inside the pores is, of course, thicker than the film on the flat surface. The values of velocity are determined from the time of flight of the point of maximum amplitude on the received third-sound pulse. Very near the transition, the third-sound pulse is broad, and for $h_N \approx D_c$ the leading edge of the pulse is insensitive to changes in film thickness. This would suggest that the temporal position of the pulse peak is not a particularly good measure of third-sound velocity because a diffusive component may be present.

In spite of this, it is interesting to determine σ_s from the third-sound measurements (even though a diffusive mode is likely present). Using $\sigma_s=\langle\rho_s\rangle h$ and Eq. (3) for the third-sound velocity on the smooth substrate, we have

$$\frac{\sigma_s}{T_c}=\frac{C_3^2}{3\alpha}\frac{\rho h_N^4}{(1+TS/L)^2T_c} . \tag{23}$$

C_3 and the thickness h_N on Nuclepore are determined as described earlier. The expression for the velocity given in Eq. (3) is not valid for the porous Nuclepore; we must include the index of refraction for Nuclepore. This gives for the porous substrate

$$\frac{\sigma_s}{T_c}=\frac{C_3^2 n^2 \rho h_N^4}{3\alpha(1+TS/L)^2T_c} . \tag{24}$$

A plot of σ_s/T as a function of thickness on Nuclepore deduced from measurements of C_3 is shown in Figs. 18(a) and 18(b) for the nonporous and the 2000-Å Nuclepore, respectively. For the thickness values $h_N \leq 6$, the plateau value of the index shown in Fig. 11(a), $n=2.7$, has been used. Error bars based on the error in determining the third-sound time of flight are included in the figure. Above the transition, σ_s/T is linear as expected; the slope should be equal to ρ_s/T for the given temperature. The solid line in Fig. 18(a) shows the expected slope, which is consistent with the data at low coverages; at higher coverages retardation effect become increasingly important. Both the nonporous and the porous Nuclepore show continuous transitions; in fact, the porous Nuclepore appears to have a sharper transition that the nonporous Nuclepore, contrary to expectations and observations on other porous substrates. A rough estimate of the transition thickness can be obtained from the peak in the third-sound velocity. Using this criteria, the transitions occur at the flat thickness values $h_N \approx 4.95$ and $h_N \approx 5.2$ atomic layers for the porous and the nonporous substrate, respectively; both transitions occur at $\sigma_s/T_c \sim 3.5\times10^{-9}$ gm/cm^2 K. Although on Nuclepore the transitions apparently occur at different thicknesses on the porous and the nonporous substrate, this is not the case for packed powder of different grain sizes. For ^{4}He adsorbed on a

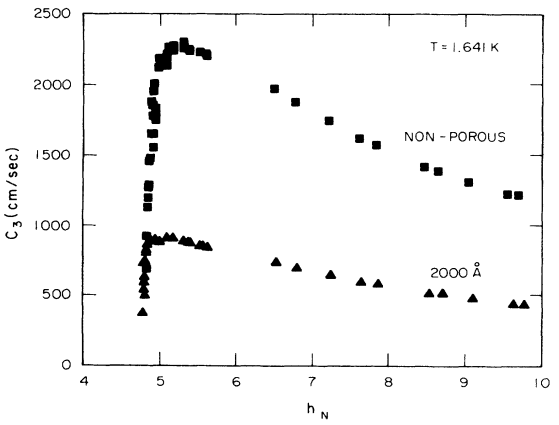

FIG. 17. Third-sound velocity as a function of film thickness on Nuclepore. Squares denote the nonporous Nuclepore, triangles denote the 2000-Å-diameter Nuclepore. The peak in the velocity is at slightly lower film thickness for the porous substrate than for the nonporous substrate. h_N is the film thickness determined from Eq. (19) or, for the porous case, is the film thickness in the pore as determined from Eq. (9).

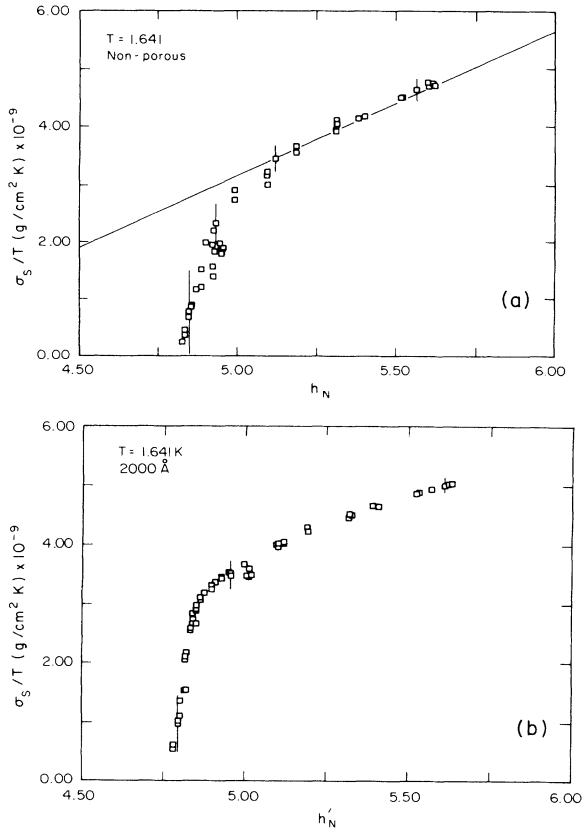

FIG. 18. (a) σ_s/T for the nonporous Nuclepore as a function of Nuclepore film thickness [assuming $\alpha_N=50$ (layers)^3 K]. (b) σ_s/T for the 2000-Å Nuclepore as a function of Nuclepore film thickness. The transition appears to be sharper on the porous substrate than on the nonporous substrate, and seems to occur at a lower coverage.

sphere, Kotsubo and Williams predict the transition thickness to be independent of the sphere radius. This prediction is confirmed by their experiments with 1 μm, 3000-, and 500-Å packed powder.[29] It thus appears that the presence of the pores in Nuclepore affects both the position and shape of the superfluid transition, while in packed powder only the shape is affected. Further work using a third-sound resonator and Nuclepore of several pore diameters is underway to examine this.

IV. CONCLUSIONS

We have observed hysteresis in the adsorption and desorption of ^{4}He adsorbed on Nuclepore of 800- and 2000-Å pore diameters. The hysteresis cannot be explained solely on the basis of a distribution in pore diameters, but is due to hydrodynamic instabilities of the ^{4}He film adsorbed in the cylindrical pore, as described by Saam and Cole.[5] We see this hysteresis both in third-sound index of refraction and in the amount of ^{4}He adsorbed as measured by a capacitive technique. To explain the detailed shape of each curve, it is necessary to assume a distribution in pore diameters. The pore distributions obtained by applying the Cohen-Guyer-Machta[3] theory to the index data are in general agreement with those obtained using the theory of Saam and Cole and the capacitance data.

In addition, we investigated the Kosterlitz-Thouless[4] transition on the 2000-Å Nuclepore in a preliminary way. In contrast to the results on other porous substrates, it appears that the transition on the porous Nuclepore is sharper than the transition on nonporous Nuclepore, and that the transition thickness is different on the two substrates. A more thorough investigation which will examine Nuclepore of several pore sizes and more precisely locate the Kosterlitz-Thouless transition using a third-sound resonator rather than the pulsed third-sound technique employed here is underway.

ACKNOWLEDGMENTS

We have benefited from numerous conversations with S. Cohen, R. Guyer, J. Machta, and J. Valles, Jr. D. Peterson, Nuclepore Corporation, kindly provided us with information concerning Nuclepore filter fabrication and his understanding of the pore geometry early in this work. We are indebted to Mr. Robert Verner for superb craftsmanship in the fabrication of various apparatus components. This work was supported by the National Science Foundation under Grant Nos. DMR 83-18054 and DMR 85-17939.

---

[1]Nuclepore Corporation, Pleasanton, CA.

[2]J. M. Valles, Jr., D. T. Smith, and R. B. Hallock, Phys. Rev. Lett. **54**, 1528 (1985).

[3]S. Cohen, R. A. Guyer, and J. Machta, Phys. Rev. B **33**, 4664 (1986).

[4]J. M. Kosterlitz and D. J. Thouless, J. Phys C **6**, 1181 (1973).

[5]W. F. Saam and M. W. Cole, Phys. Rev. B **11**, 1086 (1975).

[6]T. P. Chen, M. J. DiPirro, A. A. Gaeta, and F. M. Gasparini, J. Low. Temp. Phys. **26**, 927 (1977).

[7]E. A. Flood, *The Solid-Gas Interface* (Dekker, New York, 1967).

[8]W. C. Tomlinson, G. G. Ihas, and F. Pobell, Phys. Rev. B **11**, 4292 (1975).

[9]J. S. Brooks, B. B. Sabo, P. C. Schubert, and W. Zimmerman, Jr., Phys. Rev. B **19**, 4524 (1979).

[10]E. S. Sabisky and C. H. Anderson, Phys. Rev. A **7**, 790 (1983).

[11]See S. Putterman, *Superfluid Hydrodynamics* (North-Holland, Amsterdam, 1974), Chap. V.

[12]The empirical form for $\langle \rho_s \rangle / \rho$ was reported in J. H. Sholtz, E. O. McLean and I. Rudnick, Phys. Rev. Lett. **32**, 147 (1974). In this reference T should be removed from the expression for D. [See I. Rudnick in *New Directions in Physics Acoustics, LXIII Corso* (Society Italiana di Fisica, Bologna, Italy, 1976), p. 112.]

[13]D. Bergman, Phys. Rev. **188**, 370 (1969); Phys. Rev. A **3**, 2058 (1971); and R. K. Galkiewicz, K. L. Telschow, and R. B. Hallock, J. Low Temp. Phys. **26**, 147 (1977).

[14]See, for example, V. Kotsubo and G. A. Williams, Phys. Rev. Lett. **53**, 691 (1984), for measurements of $D(T)$ on Al_2O_3 powder and D.T. Smith and R. B. Hallock, Phys. Rev. B **34**, 226 (1986) for $D(T)$ on Si.

[15]D. D. Awschalom, J. Warnock, and M. W. Shafer, Phys. Rev. Lett. **57**, 1607 (1986).

[16]S. J. Gregg and K. S. W. Sing, *Adsorption, Surface Area, and Porosity* (Academic, New York, 1967), Chaps. 3 and 4.

[17]1958 He Scale of Temperatures, N. B. S. Monograph 10 (1960).

[18]We use an MKS Baratron differential pressure gauge (model 145BH-10).

[19]I. Rudnick, R. S. Kagawada, J. C. Fraser, and E. Guyon, Phys. Rev. Lett. **20**, 430 (1968).

[20]Silver Print, GC Electronics, Rockport, IL.

[21]We used a Biomation transient recorder (model 805) and a Nicolet signal averager (model 1073).

[22]Several earlier studies at this laboratory [D. T. Smith, M. Liebl, M. D. Bummer, and R. B. Hallock, in *Proceedings of the XVII International Conference on Low Temperature Physics,* edited by V. EcKern *et al.* (North-Holland, Amsterdam, 1984), p. 57; and D. T. Smith and R. B. Hallock, Phys. Rev. B **34**, 226 (1986)] have seen a thickness-dependent index of refraction between a rough and smooth substrate which can be related to the length scale of that roughness using the CGM theory described earlier in this work. The first reference reports an index for glass dusted with 0.3-micron diameter alumina powder which is very similar to the data of Fig. 5. In the second reference, data on the index versus film thickness accurately predicts the length scale of the roughness of an etched silicon wafer.

[23]David R. Nelson and J. M. Kosterlitz, Phys. Rev. Lett. **39**, 1201 (1977).

[24]J. Maps and R. B. Hallock, Phys. Rev. B **28**, 4021 (1983).

[25]I. Rudnick and J. C. Fraser, J. Low Temp. Phys. **3**, 225 (1970).

[26]I. Rudnick, Phys. Rev. Lett. **40**, 1454 (1978).

[27]V. Ambegaokar, B. I. Halperin, D. R. Nelson, and E. D. Siggia, Phys. Rev. B **21**, 1806 (1980).

[28]D. J. Bishop and J. D. Reppy, Phys. Rev. Lett. **40**, 1727 (1978).

[29]V. Kotsubo and G. A. Williams, Phys. Rev. B **33**, 6106 (1986).

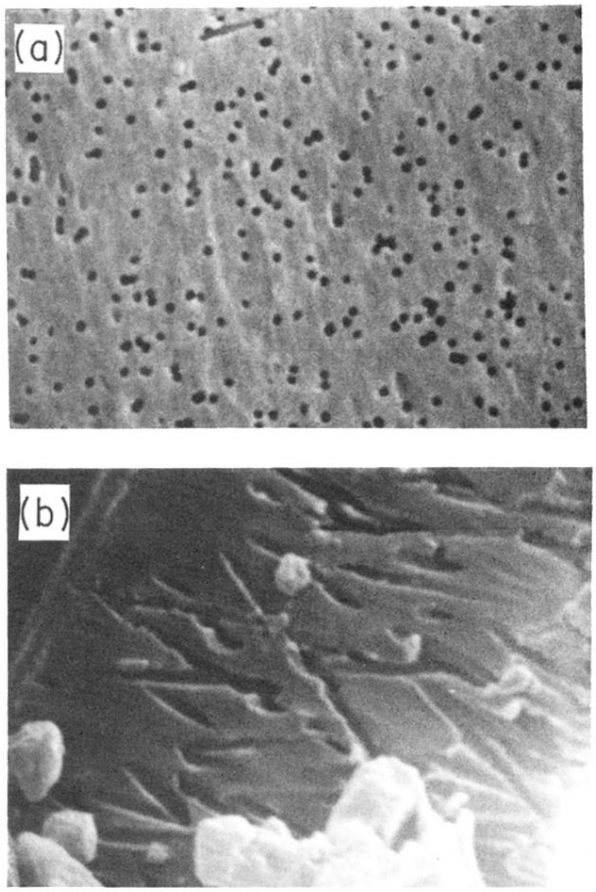

FIG. 2. Scanning electron microscope pictures of (a) the surface and (b) the cross section of a 2000-Å Nuclepore sample prepared by low-temperature microtome. Both pictures were taken after sputtering ~ 200 Å of Pt onto the surfaces. Samples were also prepared with 500, 1000, and 1500 Å of Ag evaporated onto the surface; measurements of the pore opening dimensions for these samples showed that the Ag did not measurably decrease the diameter of the pore openings.